
A Kolmogorov-Arnold Network for Interpretable Cyberattack Detection in AGC Systems

Jehad Jilan¹ Niranjana Naveen Nambiar¹ Ahmad Mohammad Saber¹ Alok Paranjape¹
Amr Youssef² Deepa Kundur¹

¹University of Toronto

²Concordia University

Abstract

Automatic Generation Control (AGC) is essential for power grid stability but remains vulnerable to stealthy cyberattacks, such as False Data Injection Attacks (FDIAs), which can disturb the system's stability while evading traditional detection methods. Unlike previous works that relied on black-box approaches, this work proposes Kolmogorov-Arnold Networks (KAN) as an interpretable and accurate method for FDIA detection in AGC systems, considering the system nonlinearities. KAN models include a method for extracting symbolic equations, and are thus able to provide more interpretability than the majority of machine learning models. The proposed KAN is trained offline to learn the complex nonlinear relationships between the AGC measurements under different operating scenarios. After training, symbolic formulas that describe the trained model's behavior can be extracted and leveraged, greatly enhancing interpretability. Our findings confirm that the proposed KAN model achieves FDIA detection rates of up to 95.97% and 95.9% for the initial model and the symbolic formula, respectively, with a low false alarm rate, offering a reliable approach to enhancing AGC cybersecurity.

Keywords: Automatic Generation Control, Kolmogorov-Arnold network, cyber-physical security, machine learning

1 Introduction

Automatic Generation Control (AGC) systems are a vital component of modern power generation, automatically balancing demand and supply by receiving measurements from across the network. Their connectivity and critical role also make them attractive targets for cyberattacks [12]. For example, in 2007, the Idaho National Laboratory demonstrated a vulnerability in network communication protocols that allowed repeated opening of a generator's circuit breakers out of sync with the grid, ultimately destroying the generator [25]. Similarly, in 2015, a cyberattack on Ukraine's power grid via the Supervisory Control and Data Acquisition (SCADA) system, a subsection of AGC, opened breakers in substations across the network and left hundreds of thousands without power [6]. Such incidents underscore the severe economic and human impacts of power system attacks, and the need for effective detection mechanisms [18].

Conventional model-based FDIA detection methods often ignore AGC nonlinearities, limiting their practicality [19]. In contrast, machine learning (ML) approaches can directly handle nonlinear and temporal patterns in measurements without abstraction [2]. Prior works [14] explored neural net-

works and autoencoders such as Multi-Layer Perceptrons (MLPs) [5], LSTM autoencoders [2], and related classifiers [19], but these models largely function as black boxes. Their lack of interpretability undermines operator trust in critical infrastructure applications [15, 20, 22]. For domains where cyberattacks can bypass traditional security measures, interpretability becomes crucial: operators must understand the cause-and-effect relationships behind a model’s outputs to make informed and trustworthy decisions [10, 13].

This paper presents a new interpretable learning-based method for FDIA detection in AGC systems that explicitly considers AGC nonlinearities. The approach leverages Kolmogorov-Arnold Networks (KANs), recently proposed ML models [10], which approximate symbolic expressions at each internal node as multivariate equations representing learned relationships. Through training, pruning, and fine-tuning, a KAN yields an accurate detection model, followed by symbolification to extract interpretable mathematical expressions. These expressions provide transparent, human-readable decision rules for detecting FDIAs in AGC measurements, enhancing trust compared to existing black-box methods.

2 Preliminaries and Threat Model

AGCs are centralized control systems that maintain frequency and system stability across power grids. Disturbances, whether legitimate events such as load changes, generator outages, or equipment failures, or malicious cyberattacks, cause deviations in operating parameters such as frequency and tie-line power flow. In response, each area’s measurements are sent to the control center [19], as shown in Fig. 2.1. To regulate generator outputs and ensure balanced inter-area power exchange and supply-demand equilibrium [19, 23], AGC then computes the Area Control Error (ACE):

$$ACE = \Delta P_{tie} + B\Delta f \tag{2.1}$$

where ΔP_{tie} is the mismatch between scheduled and actual tie-line power interchange, Δf is the frequency deviation, and B is the area’s frequency bias factor [23]. The AGC controller drives the ACE toward zero [7], thereby maintaining safe tie-line flows and stabilizing system frequency [7, 23]. AGC systems also exhibit inherent nonlinearities that affect their response to disturbances [19]. These include the Governor Dead Band (GDB), which ignores small frequency variations (about 0.5 Hz) to prevent excessive turbine valve movements and mechanical wear [16, 19]; the Generation Rate Constraint (GRC), a physical limit on the rate of change of generator output (typically 3% per minute in thermal plants), which preserves equipment longevity and filters manipulations within the bound [9]; and Transport Delays, arising from communication latency and mechanical responses, which create windows during which attacks may go undetected [2]. As cyber-physical systems [22], AGCs rely on communication protocols such as Distributed Network Protocol 3 (DNP3) [1], making their measurement signals vulnerable to manipulation. False Data Injection Attacks (FDIAs) exploit this vulnerability by stealthily altering transmitted measurements [19]. Attackers typically apply gradual, coordinated manipulations, implemented as ramp, pulse, or step functions, that bypass conventional bad-data detection, which only flags large anomalies based on residual thresholds [19, 22]. By exploiting system tolerances, such perturbations appear indistinguishable from normal fluctuations, especially when viewed at a single snapshot in time, where small deviations resemble noise [22]. This makes FDIA detection particularly challenging. To address these threats, detection methods must satisfy three requirements. They must account for inherent AGC nonlinearities, capture the temporal evolution of attacks that unfold gradually across multiple time steps, and provide interpretable outputs that allow operators to understand the rationale behind each detec-

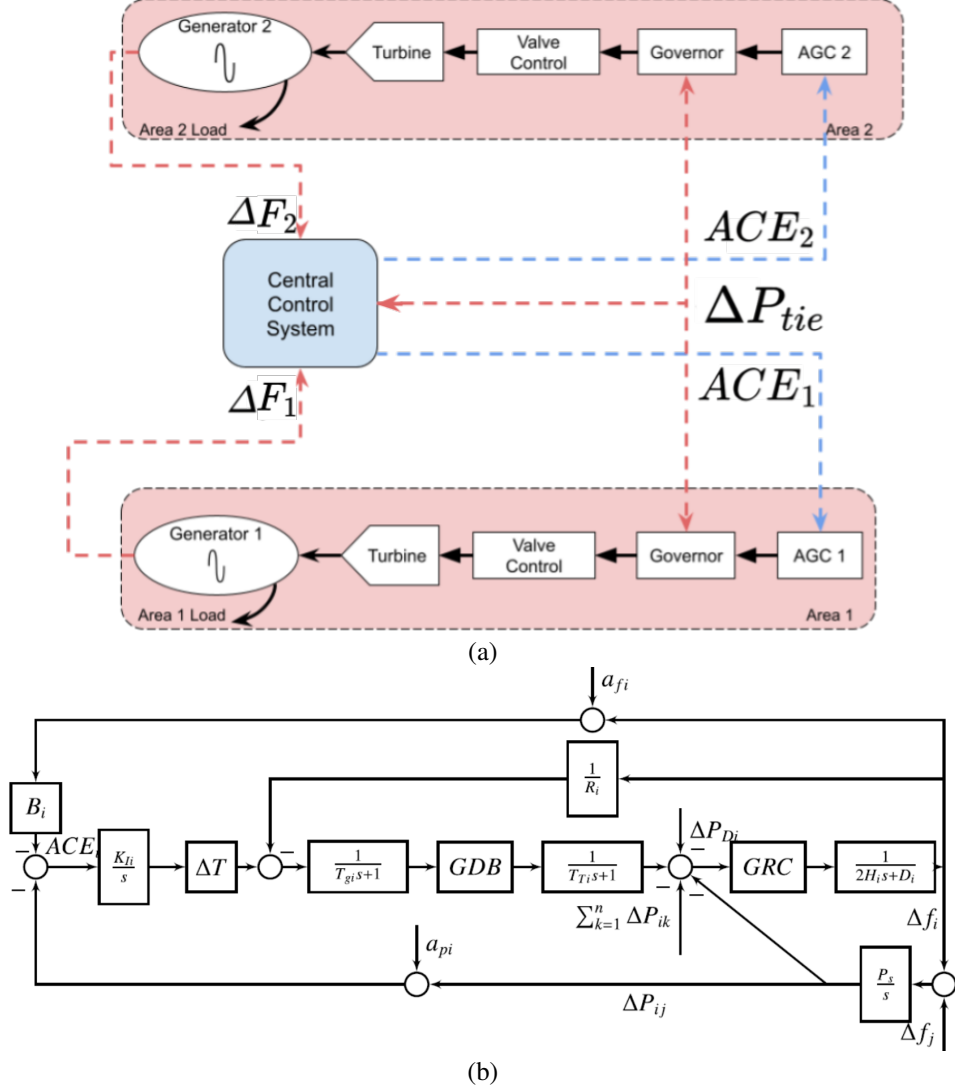


Figure 2.1: AGC system controlling a two-area power system, (a) information flow, (b) block diagram representation of inherent AGC nonlinearities [19]

tion decision. This paper proposes an interpretable AI model that distinguishes between normal and attacked AGC measurements, as explained in the next section.

3 Proposed Solution's Methodology

3.1 KANs for FDIA Detection in Non-linear AGC Systems

Kolmogorov-Arnold Networks (KANs), illustrated in Fig. 3.1, are a recently introduced alternative to multilayer perceptrons (MLPs), designed to provide interpretable models that expose underlying mathematical structures [10]. In this work, KANs are used as the interpretable AI framework to distinguish between normal and attacked AGC measurements. Through a process known as *symbolification*, which employs the `auto_symbolic` method, KANs extract human-readable symbolic expressions $\xi(x)$ that approximate how input features influence decisions. This transparency enables operators to understand and trust the model's logic when detecting attacks [17].

KANs are grounded in the Kolmogorov-Arnold theorem, which states that any multivariate continuous function can be decomposed into a finite sum of univariate functions:

$$\Psi_{k,l} : [0, 1] \rightarrow \mathbb{R}, \quad \Phi_k : \mathbb{R} \rightarrow \mathbb{R} \quad (3.1)$$

$$F(x) = \sum_{k=1}^{2n+1} \Phi_k \left(\sum_{l=1}^n \Psi_{k,l}(x_l) \right) \quad (3.2)$$

where $F : [0, 1]^n \rightarrow \mathbb{R}$. This formulation allows high-dimensional functions to be approximated by sums of univariate transformations, making KANs suitable for modeling the nonlinear patterns in AGC sensor data.

The original representation, however, has limited expressiveness due to its shallow, fixed structure. Modern KANs extend this framework to deeper architectures with arbitrary widths and depths, enabling the modeling of high-dimensional, nonlinear, and non-smooth functions. In matrix form, for input vector x , a KAN layer is defined as

$$F(x) = \Omega_{out} \circ \Omega_{in} \circ x \quad (3.3)$$

where

$$\Omega_{in} = \begin{pmatrix} \Psi_{1,1}(\cdot) & \cdots & \Psi_{1,n}(\cdot) \\ \vdots & \ddots & \vdots \\ \Psi_{2n+1,1}(\cdot) & \cdots & \Psi_{2n+1,n}(\cdot) \end{pmatrix} \quad (3.4)$$

$$\Omega_{out} = (\Phi_1(\cdot), \dots, \Phi_{2n+1}(\cdot)) \quad (3.5)$$

The output of a T -layer KAN is then

$$\text{KAN}(\mathbf{x}) = (\Omega_{T-1} \circ \Omega_{T-2} \circ \cdots \circ \Omega_0) x \quad (3.6)$$

Unlike MLPs, where weights lie on edges and fixed activation functions (e.g., ReLU) reside on nodes, KANs assign learnable univariate activation functions—parameterized as B-splines—to edges, while nodes perform summations. B-splines, piecewise polynomial functions defined over a grid, offer accurate approximations of 1D functions [10]. Their resolution can be refined by increasing grid points, allowing KANs to flexibly model diverse continuous functions [3]. Since raw B-spline coefficients are not easily interpretable, KANs employ the `auto_symbolic` method [8], which fits learned splines to commonly understood symbolic functions (e.g., sine, exponential) from a predefined library. This approximation provides explicit, human-readable expressions of input–output relationships [15], thereby enabling interpretability absent in MLPs, where activations are fixed and already in symbolic form. By leveraging this symbolification process, operators gain insight into why an event is flagged as an attack, including which input features dominate, how they interact, and the functional forms governing these relationships [11]. This interpretability enhances operator trust and supports auditing of anomaly detection logic.

3.2 Pruning and Fine-Tuning

Pruning reduces computational complexity by removing low-weight edges below a predefined threshold [24]. This simplifies the network, enhances interpretability, and improves generalization by highlighting the most influential features and relationships. However, excessive pruning can degrade performance. To mitigate this, fine-tuning retrains the pruned network, often with adjusted hyperparameters, restoring accuracy while maintaining reduced complexity. This introduces a trade-off between efficiency and the fidelity of $\xi(x)$, requiring careful balance.

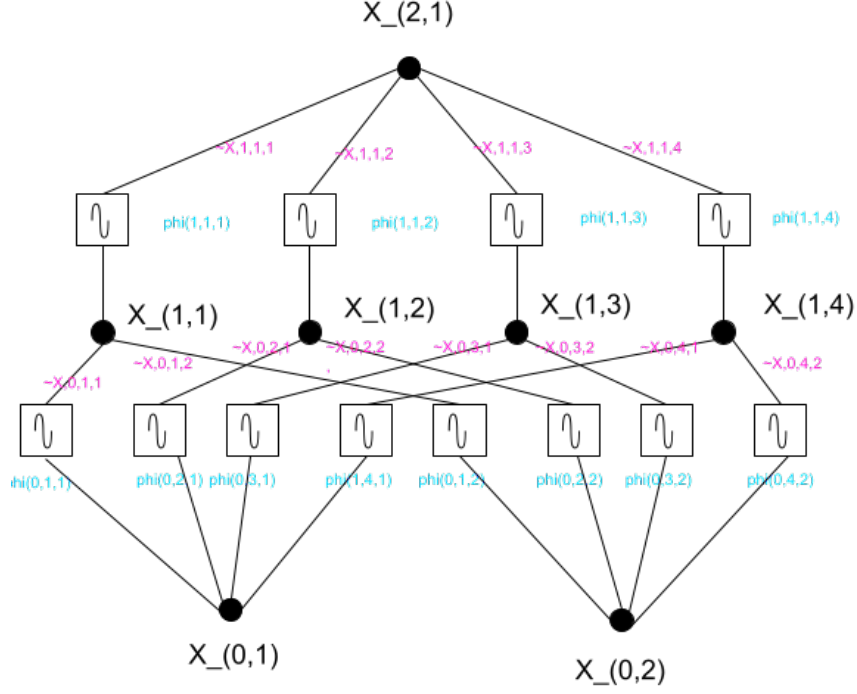


Figure 3.1: Illustration of KANs

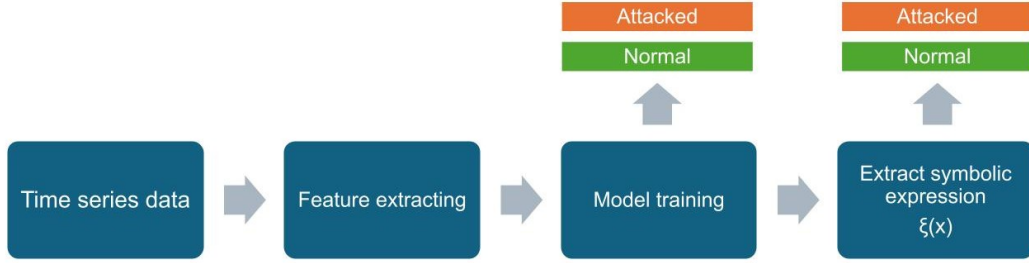


Figure 3.2: Proposed solution information flow diagram

3.3 Feature Extraction

To enable KANs to capture meaningful patterns, raw 3D time-series data are transformed into a structured 2D feature matrix. For each sample, time-series data

$$X_{ij} = [x_{i1}, x_{i2}, \dots, x_{iT}] \quad (3.7)$$

are mapped into interpretable feature vectors using a library of standard descriptors. These features quantify statistical properties, frequency-domain behavior, nonlinear dynamics, and temporal structure, as outlined in [19]. Formally,

$$\varphi = [\varphi_1, \varphi_2, \dots, \varphi_T] \quad (3.8)$$

$$\varphi(X_i) = [\varphi_1(X_i), \varphi_2(X_i), \dots, \varphi_T(X_i)] \quad (3.9)$$

producing a structured feature set (X features $\times Y$ time steps) per measurement. Fig. 3.2 shows the full processing workflow.

4 Results

4.1 Dataset Generation and Feature Extraction

A comprehensive dataset is generated using a simulated two-area AGC system model. Each sample represents a 60-second window divided into 300 time steps (duration of timestep = 0.2 seconds) for each of the three key measurements: the power flow in the tie-line (ΔP_{tie}), the change in frequency in Area 1 (ΔF_1), and the change in frequency in Area 2 (ΔF_2), sampled at 5 samples per second. Fig. 4.1 shows the time-series plots for the attacked and non-attacked simulations of these three measurements. In these plots, the blue line represents the non-attacked signal, while the red line indicates the attacked scenario. The implemented attacks are not inherently stealthy, but they exploit system tolerances through small, gradual perturbations. This time-series structure enables the model to learn characteristic attack patterns, such as ramps, scaling, or combined distortions (which simultaneously affect multiple signals) on one or more of the three AGC signals. The dataset comprises 20,000 labeled samples, distributed equally across attacked and non-attacked scenarios. To enable practical model training, six statistical features—which include mean, standard deviation, minimum, maximum, skewness, and kurtosis—are extracted from each variable within a sample, resulting in 18 features per sample. This dataset provides a benchmark for evaluating the KAN model’s ability to effectively distinguish between normal and attacked conditions in power system control scenarios.

4.2 Performance Evaluation Criteria and Metrics

The performance of the proposed KAN-based detection framework is assessed using the following metrics:

$$\text{Accuracy} = \frac{TP + TN}{TP + TN + FP + FN} \quad (4.1)$$

$$\text{Recall} = \frac{TP}{TP + FN} \quad (4.2) \quad \text{Precision} = \frac{TP}{TP + FP} \quad (4.3)$$

$$\text{F1-score} = 2 \times \frac{\text{Precision} \times \text{Recall}}{\text{Precision} + \text{Recall}} \quad (4.4)$$

where True Positives (TPs) denote correctly detected FDIAs, True Negatives (TNs) represent correctly identified normal disturbances, False Positives (FPs) are false alarms, and False Negatives (FNs) correspond to undetected FDIAs. During training, both training and validation accuracies are computed after each iteration to monitor convergence and guide weight updates during forward and backward propagation. Following training, the model’s final performance is evaluated on a separate test set.

4.3 KAN Model Training

To train and evaluate the KAN model, the dataset is split after the feature extraction stage using a 60-20-20 ratio: 60% for training, 20% for validation, and 20% for testing. The dataset is shuffled to ensure a random distribution of samples across the training, validation, and testing sets, which prevents temporal bias and ensures that the KAN model does not learn patterns based on the order of data collection. The model architecture consists of one hidden layer and a single output layer for binary classification (determining whether the system is under attack, indicated by 1, or operating normally, indicated by 0). The training process involves two primary stages: model training and the

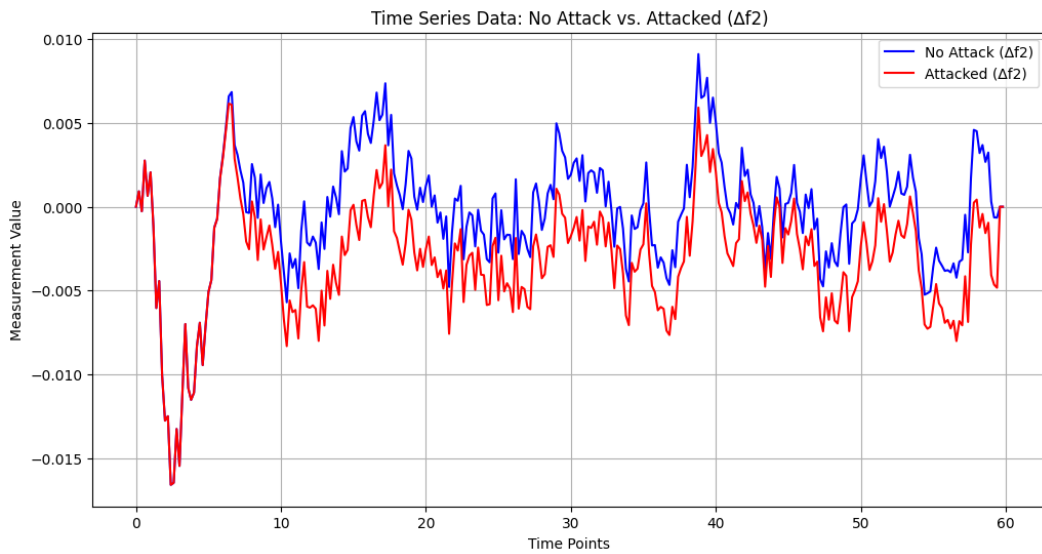
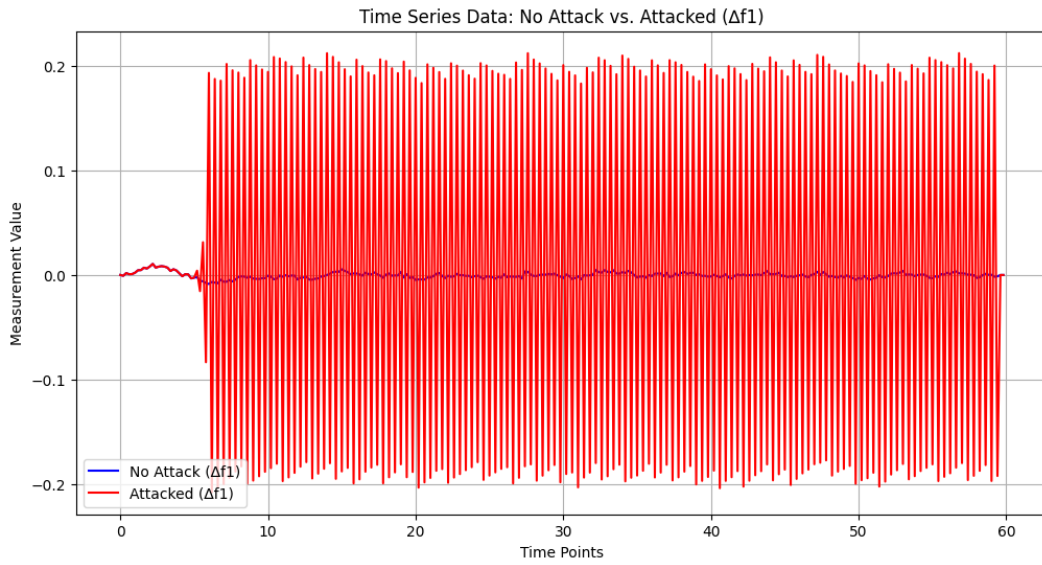
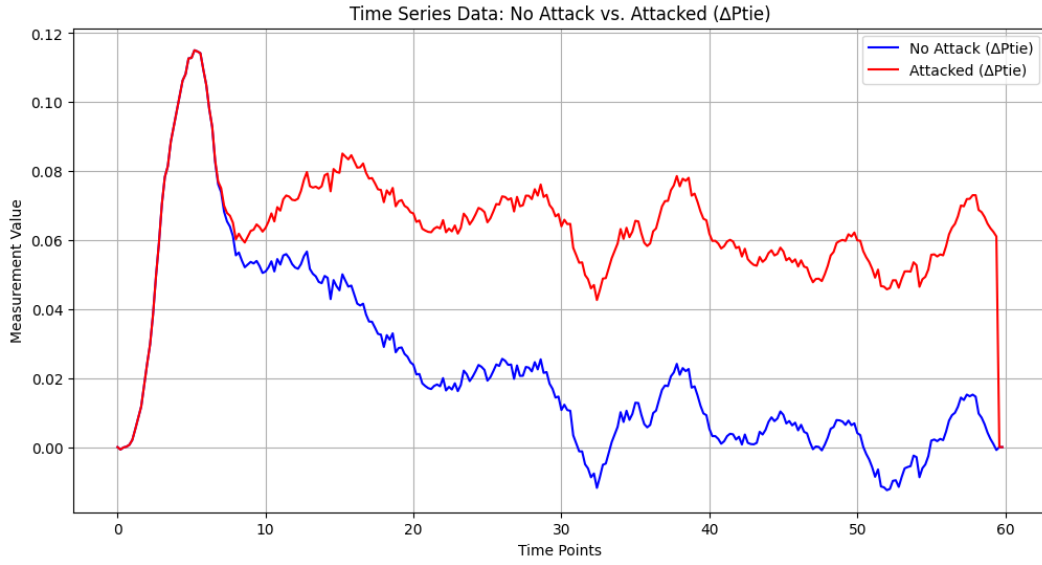


Figure 4.1: AGC measurements under a normal disturbance and an FDIA

Approach	TPs	TNs	FPs	FNs
KAN Model	49.03%	48.25%	0.98%	1.75%
$\xi(x)$	37.08%	46.48%	12.93%	3.53%

Table 1: Confusion matrix for Experiment 1

Variable x_i	Input feature $\varphi(X_i)$	Variable x_i	Input feature $\varphi(X_i)$
x_1	mean of ΔP_{tie}	x_{10}	max of ΔF_1
x_2	std of ΔP_{tie}	x_{11}	skew of ΔF_1
x_3	min of ΔP_{tie}	x_{12}	kurtosis of ΔF_1
x_4	max of ΔP_{tie}	x_{13}	mean of ΔF_2
x_5	skew of ΔP_{tie}	x_{14}	std of ΔF_2
x_6	kurtosis of ΔP_{tie}	x_{15}	min of ΔF_2
x_7	mean of ΔF_1	x_{16}	max of ΔF_2
x_8	std of ΔF_1	x_{17}	skew of ΔF_2
x_9	min of ΔF_1	x_{18}	kurtosis of ΔF_2

Table 2: Extracted features and corresponding variables in $\xi(x)$

extraction of the symbolic expression $\xi(x)$. During training, we utilize the KAN model, employing "LBFGS" as the optimizer and binary cross-entropy with logits loss as the criterion, and the model is trained for 50 epochs [8]. The accuracy of both the model and the extracted approximate expression is measured using the same evaluation metrics to ensure comparability.

4.4 Extracting Symbolic Expression $\xi(x)$

To extract an interpretable symbolic expression $\xi(x)$, a predefined library of common mathematical functions is applied, as described in [8]. This library, 'lib', includes x , x^2 , x^3 , x^4 , exp, log, $\sqrt{\cdot}$, tanh, sin, tan, and $|\cdot|$, covering polynomial, transcendental, trigonometric, and absolute value functions to effectively capture nonlinear relationships in control systems. Using the symbolification process with the auto_symbolic method, the learned numerical B-splines are iteratively fitted to functions in 'lib' to obtain the approximate symbolic expression $\xi(x)$. The resulting expression is then evaluated on the test dataset to compute predictions for each trial.

4.5 KAN Model Testing Results

In this subsection, we discuss the results of two KAN models and their corresponding extracted symbolic expressions, obtained through two training experiments.

4.5.1 Experiment 1: Model Training without Pruning

In the first experiment, we evaluating the trained model on the test dataset. Our results demonstrate that the proposed KAN achieves an accuracy of 97.28% (test accuracy), as shown in the corresponding confusion matrix presented in Table 1. Based on the distribution of the confusion matrix, the extracted expression $\xi(x)$ achieves an accuracy of 83.55%, indicating a 13.73% difference in test accuracy compared to the original KAN model. These results suggest that the initial extracted expression $\xi(x)$ does not fully capture the model's performance. This inherent discrepancy between the KAN model and its extracted symbolic expression exists [15] because learned splines are piecewise polynomial functions optimized for local behaviours across specific grids [21], while 'lib' contains global, candidate symbolic functions [8]. When the learned splines represent relationships that do not match the available functions in 'lib', $\xi(x)$ inherently becomes a less accurate approximation of the original spline representation [10].

$$\xi(x) = -0.0585980133191944x_1 + 0.000117332582424649x_{10} - 0.0032927613617984x_{11} + 0.199718993320776x_{13} + 1.55716813155639x_{14} - 0.385990369544651x_{15} - 0.0448305190728965x_{16} + 0.00274879548492894x_{17} - 7.26539041831069x_{18} + 1.97461899547397x_2 - 0.379653532778621x_3 - 0.0754184456757745x_4 - 0.000456697049837721x_5 - 0.0128194429255578x_6 - 0.191752437447404x_7 + 0.00114824399675933x_8 - 0.968688987037606x_9 - 0.00883291241612655(-0.468704782289004x_{13} - 1)^2 - 4.72708101348157 \sin(0.957720279693604x_{10} - 3.32732892036438) + 5.73315222012583 \sin(0.555177330970764x_{11} + 4.43385314941406) + 32.7409959816164 \sin(0.174312055110931x_{12} + 8.20001411437988) + 0.0035802557051504 \sin(0.956642866134644x_{12} + 5.17221975326538) - 12.1630349406289 \sin(0.998832166194916x_{17} - 4.81406164169312) - 4.26815155798069 \sin(1.73705363273621x_5 + 4.22196102142334) + 23.7266100016899 \sin(0.378205478191376x_6 - 1.20097088813782) - 0.000351969165512922 \sin(1.46384525299072x_7 + 2.60268974304199) + 0.000128227534902977 \sin(1.68783116340637x_9 - 9.2935266494751) + 3.77017307281494 \sin(0.0843539329592812x_1 + 0.238444275174417x_{12} + 0.0462676948760776x_{14} + 0.0923445399265967x_{15} - 0.0580918728556772x_{16} + 0.0951570508621111x_2 + 0.0741397094775877x_3 - 0.0539274457533548x_4 + 0.107240936394151x_7 + 0.180578023398408x_8 + 0.0949108993126466x_9 + 0.277275392577905(-0.421461460872531x_{13} - 1)^2 + 1.28023221870478(-0.779671045641072x_5 - 1)^2 + 0.0752890894790301 \sin(0.716302752494812x_{10} - 8.49989604949951) - 1.20668354318268 \sin(0.332572400569916x_{11} - 4.27891731262207) - 0.67718796920569 \sin(1.32690954208374x_{17} - 2.76635670661926) - 0.0658867057632451 \sin(1.41109359264374x_{18} - 5.204674243927) - 0.209507586992645 \sin(0.44487389922142x_6 - 1.19521081447601) - 0.521033729786071) - 0.94885917663574 \sin(-0.0430169017268552x_{14} + 0.1759948950534x_{17} + 0.125936817687353x_{18} + 0.0905268996409984x_3 - 0.241044177965138x_5 + 0.0423055128500324x_7 + 0.0670621236298565x_9 + 0.168459767760968(1 - 0.640183528357079x_8)^2 + 0.456006958196413(-0.18530568784075x_{13} - 1)^2 + 0.0201138477256463 \sin(0.276036202907562x_1 - 1.07064199447632) + 0.0306207115979236 \sin(0.703351020812988x_{10} + 3.88148498535156) + 1.0628759872633 \sin(0.19111530482769x_{11} + 4.97953748703003) + 3.08240806358086 \sin(0.378823727369308x_{12} + 5.19191455841064) - 0.0016931647372771 \sin(1.57478618621826x_{15} - 9.01122283935547) - 0.056193512054481 \sin(0.303063929080963x_{16} - 4.35543346405029) - 0.0265940280273071 \sin(1.05447638034821x_2 - 5.42998838424683) - 0.00954213252204161 \sin(0.631563544273376x_4 + 0.770899593830109) - 0.532747695217815 \sin(0.431170105934143x_6 + 5.20463800430298) + 11.1773035489992) + 0.209164789502615 \tan(1.01208245754242x_8 - 1.01426601409912) + 16.8226771911957$$

Figure 4.2: Extracted symbolic expression from the trained KAN model in Experiment 2

Approach	TPs	TNs	FPs	FNs
KAN Model	48.3%	47.68%	1.7%	2.33%
$\xi(x)$	47.75%	48.15%	2.25%	1.85%

Table 3: Confusion matrix for Experiment 2

Experiment	Approach	Accuracy	Precision	Recall	F1-score
1	KAN model	97.28%	98.02%	96.5%	97.25%
1	$\xi(x)$	83.55%	78.24%	92.95%	84.96%
2	KAN model	95.97%	96.56%	95.35%	95.95%
2	$\xi(x)$	95.9%	95.54%	96.3%	95.92%

Table 4: Performance metrics for KAN model and associated $\xi(x)$ across experiments

4.5.2 Experiment 2: Model Training, Pruning and Fine-Tuning

In this experiment, the training method follows the approach described in [4]. The method applies pruning followed by fine-tuning of the model to reduce the discrepancy between the model’s accuracy and that of our extracted approximated expression $\xi(x)$, shown in Fig. 4.2. Note that each x_i in the symbolic expression represents an Feature as shown in Table 2. Applying the sigmoid activation function to $\xi(x)$ then maps the continuous output into the range $[0, 1]$, where a threshold of 0.5 classifies the signal as either normal (≤ 0.5) or attacked (> 0.5). By applying pruning and fine-tuning, the accuracy of the model reduces to 95.97%, while the accuracy of $\xi(x)$ increases to 95.9%. Table 3 shows the confusion matrices corresponding to the accuracy of our model and the approximated extracted expression $\xi(x)$. This method reduces the difference between the two accuracies from 13.73% to 0.07%.

4.5.3 Discussion

Table 4 shows the summary results of 2 experiments: 1) training the KAN model without pruning, and 2) training the KAN model, pruning it, and fine-tuning it. From the power system operation perspective, the most crucial efficiency is to reduce the false alarm rate while keeping the attack detection high to ensure that no false alarms trigger unnecessary control actions that could compromise

system stability. The KAN model in Experiment 1 achieves a high accuracy of 97.28%, with low false alarm rates, strong attack detection capability, and a high F1-score of 97.25%. These results demonstrate high classification performance, effectively balancing precision and recall. However, after extracting the approximate symbolic expression $\xi(x)$ in Experiment 1, the performance of $\xi(x)$ shows a decline across all metrics, particularly in precision for attack detection, which drops to 78.24%. The overall accuracy falls to 83.55%, representing a 13.73% decrease compared to the original model. This result highlights the reduced effectiveness of the initial $\xi(x)$ in approximating the model’s decision threshold. In Experiment 2, after applying pruning and fine-tuning, the KAN model maintains strong performance with an accuracy of 95.97%, a precision of 96.56%, a recall of 95.35%, and an F1-score of 95.95%. While this represents a slight reduction of approximately 2% compared to the initial model for both test accuracy and F1-score, it remains robust. Notably, $\xi(x)$ ’s performance significantly improves in Experiment 2, achieving an accuracy of 95.9% and an F1-score of 95.92%. The difference between the model and $\xi(x)$ results is reduced to less than 0.1%, demonstrating that pruning and fine-tuning effectively narrow the gap between the learned model and its approximate, interpretable representation. These results demonstrate the strong capability of the KAN model to detect cyberattacks on the AGC system while maintaining a low false alarm rate. In the application of AGCs [22], instead of feature importance rankings which are provided by traditional post-hoc interpretability methods used for MLPs [10] like Local Interpretable Model-agnostic Explanations (LIME) and SHapley Additive exPlanations (SHAP), this symbolification process of KANs allows operators to approximate attack patterns as mathematical relationships [10]. For instance, following our approximate symbolic expression $\xi(x)$ extracted from the KAN model in Fig. 4.2 with Table II, operators can identify that the dominance of ΔF_2 ’s statistical features, specifically the largest magnitude coefficient of ≈ -7.27 for kurtosis (x_{18}) and the second largest positive coefficient of ≈ 1.56 for standard deviation (x_{14}), suggests that the FDIAs most significantly alter the statistical distribution of Area 2’s frequency response across all its measured characteristics. For the AGC system model that is used to generate our dataset, its Area 2 is thus more vulnerable to attacks; this insight allows operators to prioritize monitoring efforts and resource allocation there. Due to the high accuracy and interpretability that $\xi(x)$ provides, AGC operators can inspect the functions learned for each relationship, identify which specific measurement is highly targeted by the FDIA, and can trust and audit the model’s decision-making process, unlike with black-box models. Moreover, this outcome illustrates the trade-off between interpretability and model accuracy, highlighting the potential for improved symbolic approximations through targeted model optimization [10].

5 Conclusion and Future Work

This paper presented an interpretable KAN-based approach for detecting cyberattacks on AGC systems considering system nonlinearities. The proposed method achieves both high detection accuracy and a low false alarm rate, while also enabling the extraction of an approximate symbolic expression that enhances interpretability. The expression $\xi(x)$ provides a mathematical mapping from input features to classification outcomes, i.e., normal disturbance vs FDIA. We evaluated the KAN model on a comprehensive dataset containing multiple types of cyberattacks targeting three critical AGC signals. The results show that the approach delivers strong performance and interpretability: the trained KAN achieved 95.97% accuracy, while $\xi(x)$ achieved 95.9%. Future work can focus on further improving interpretability, extending the framework to attack identification in addition to detection, and developing real-time processing capabilities for practical deployment.

References

- [1] Amir Ameli, Ali Hooshyar, Ehab F El-Saadany, and Amr M Youssef. Attack detection and identification for automatic generation control systems. *IEEE Trans. Power Syst.*, 33(5):4760–4774, 2018.
- [2] Abdelrahman Ayad, Mohsen Khalaf, Magdy Salama, and Ehab F. El-Saadany. Mitigation of false data injection attacks on automatic generation control considering nonlinearities. *Electr. Power Syst. Res.*, 209:107958, 2022.
- [3] Irina Barašin, Blaž Bertalanič, Mihael Mohorčič, and Carolina Fortuna. Exploring kolmogorov-arnold networks for interpretable time series classification, 2025.
- [4] Team Daniel. Kan: Classification example notebook. Online. Available: https://github.com/team-daniel/KAN/blob/master/KAN_classification.ipynb, Accessed: Aug. 2024.
- [5] Deepchecks. Multilayer perceptron (mlp): Definition, pros and cons. Online. Available: <https://www.deepchecks.com/glossary/multilayer-perceptron/#:~:text=Black%20box%20model%E2%80%93MLPs%20are,easily%20overfit%20the%20training%20data>, Accessed: Jul. 14, 2025.
- [6] Electricity Information Sharing and Analysis Center. Analysis of the cyber attack on the ukrainian power grid. Technical report, Electricity Information Sharing and Analysis Center, Washington, DC, USA, 2016.
- [7] Tong Huang, Bharadwaj Satchidanandan, PR Kumar, and Le Xie. An online detection framework for cyber attacks on automatic generation control. *IEEE Trans. Power Syst.*, 33(6):6816–6827, 2018.
- [8] Xiaoming Kind. Pykan: Kolmogorov-arnold network in python – introduction. Online. Available: <https://kindxiaoming.github.io/pykan/intro.html>, Accessed: Aug. 2024.
- [9] Sandeep Kumar et al. Agc and avr of interconnected thermal power system while considering the effect of grc’s. *Int. J. Soft Comput. Eng.*, 2:2117–2126, 2012.
- [10] Ziming Liu, Yixuan Wang, Sachin Vaidya, Fabian Ruehle, James Halverson, Marin Soljačić, Thomas Y. Hou, and Max Tegmark. KAN: Kolmogorov-arnold networks, 2025.
- [11] Fuad Mammadzada. Design of a kolmogorov-arnold network hardware accelerator. Master’s thesis, Faculty of Engineering (LTH), Lund University, 2025.
- [12] Dimitris M. Manias, Ahmad Mohammad Saber, Mohammed I. Radaideh, Abdelrahman T. Gaber, Michail Maniatakos, Hatem Zeineldin, Davor Svetinovic, and Ehab F. El-Saadany. Trends in smart grid cyber-physical security: Components, threats, and solutions. *IEEE Access*, 12:161329–161356, 2024.
- [13] Christoph Molnar, Giuseppe Casalicchio, and Bernd Bischl. *Interpretable Machine Learning – A Brief History, State-of-the-Art and Challenges*, page 417–431. Springer, 2020.
- [14] Ahmed S. Musleh, Guo Chen, and Zhao Yang Dong. A survey on the detection algorithms for false data injection attacks in smart grids. *IEEE Trans. Smart Grid*, 11(3):2218–2234, 2020.
- [15] Nataly R. Panczyk, Omer F. Erdem, and Majdi I. Radaideh. Opening the black-box: Symbolic regression with kolmogorov-arnold networks for energy applications, 2025.

- [16] Lukumba Phiri and Simon Tembo. False data injection attacks on automatic generation control modeling and mitigation based on reinforcement learning. *Int. J. Internet Things*, 11(1):1–10, 2023.
- [17] Ahmad Mohammad Saber, Max Mauro Dias Santos, Mohammad Al Janaideh, Amr Youssef, and Deepa Kundur. A kolmogorov-arnold network for explainable detection of cyberattacks on ev chargers. *arXiv preprint arXiv:2503.02281*, 2025.
- [18] Ahmad Mohammad Saber, Amr Youssef, Davor Svetinovic, Hatem H Zeineldin, and Ehab F El-Saadany. Anomaly-based detection of cyberattacks on line current differential relays. *IEEE Trans. Smart Grid*, 13(6):4787–4800, 2022.
- [19] Nour M. Shabar, Ahmad Mohammad Saber, and Deepa Kundur. Machine learning-based cyberattack detection and identification for automatic generation control systems considering nonlinearities, 2025.
- [20] Bhagyashree Shendkar. Explainable machine learning models for real-time threat detection in cybersecurity. *Panam. Math. J.*, 35:264–275, 11 2024.
- [21] Shriyank Somvanshi, Syed Aaqib Javed, Md Monzurul Islam, Diwas Pandit, and Subasish Das. A survey on kolmogorov-arnold network. *ACM Comput. Surv.*, June 2025.
- [22] Rui Tan, Hoang Hai Nguyen, Eddy YS Foo, Xinshu Dong, David KY Yau, Zbigniew Kalbarczyk, Ravishankar K Iyer, and Hoay Beng Gooi. Optimal false data injection attack against automatic generation control in power grids. In *2016 ACM/IEEE 7th Int. Conf. Cyber-Phys. Syst. (ICCPS)*, pages 1–10, 2016.
- [23] Kaleem Ullah, Abdul Basit, Zahid Ullah, Sheraz Aslam, and Herodotos Herodotou. Automatic generation control strategies in conventional and modern power systems: A comprehensive overview. *Energies*, 14(9):2376, 2021.
- [24] xbeat. Automatic pruning of kolmogorov-arnold networks. Online. Available: <https://github.com/xbeat/Machine-Learning/blob/main/Automatic%20Pruning%20of%20Kolmogorov-Arnold%20Networks.md>, Accessed: Aug. 2024.
- [25] Mark Zeller. Myth or reality — does the aurora vulnerability pose a risk to my generator? In *2011 64th Annu. Conf. Protective Relay Eng.*, pages 130–136, 2011.